Low-temperature characterization and micropatterning of coevaporated Bi_2Te_3 and Sb_2Te_3 films

Baoling Huang,[1] Chris Lawrence,[2] Andrew Gross,[3] Gi-Suk Hwang,[1] Niloufar Ghafouri,[3] Sang-Woo Lee,[3] Hanseup Kim,[3] Chang-Peng Li,[2] Ctirad Uher,[2] Khalil Najafi,[3] and Massoud Kaviany[1,a)]

[1]*Department of Mechanical Engineering, University of Michigan, Michigan 48109, USA*
[2]*Department of Physics, University of Michigan, Michigan 48109, USA*
[3]*Department of Electrical Engineering and Computer Science, University of Michigan, Michigan 48109, USA*

(Received 13 March 2008; accepted 12 October 2008; published online 3 December 2008)

Thermoelectric (TE) properties of the coevaporated Bi_2Te_3 and Sb_2Te_3 films are measured from 100 to 300 K for Seebeck coefficient α_S and from 5 to 300 K for electrical resistivity ρ_e, mobility μ_e, and Hall coefficient R_H. For the low-temperature characterization of TE films, the conditions for coevaporation deposition of Bi, Te, and Sb to form Bi_2Te_3 and Sb_2Te_3 films are also investigated, including substrate material, substrate temperature T_{sub}, and elemental flux ratio (FR). The resublimation of Te occurring above 473 K significantly affects the film composition and quality. Our optimal deposition conditions for Bi_2Te_3 films are $T_{sub}=533$ K and FR=2.4, and those for Sb_2Te_3 films are $T_{sub}=503$ K and FR=3.0. The TE properties of both films are strongly temperature dependent, while Bi_2Te_3 films show a stronger temperature dependence than Sb_2Te_3 films due to different major scattering mechanisms. α_S of both the coevaporated films are close to or higher than those of bulk materials, but ρ_e is much higher (due to lower carrier concentrations for Sb_2Te_3 films and lower μ_e for Bi_2Te_3 films). Also, no freeze-out regime is found for both Bi_2Te_3 and Sb_2Te_3 films at low temperatures. The room-temperature power factors of α_S^2/ρ_e for Bi_2Te_3 and Sb_2Te_3 films are 2.3 and 2.0 $mW/K^2\,m$, and the maxima are 2.7 $mW/K^2\,m$ for Bi_2Te_3 at $T=220$ K and 2.1 $mW/K^2\,m$ for Sb_2Te_3 at $T=280$ K. Shadow mask technique is successfully used for the micropatterning (20 μm) of TE films with no significant change in properties. © *2008 American Institute of Physics*. [DOI: 10.1063/1.3033381]

I. INTRODUCTION

Miniature thermoelectric (TE) cryogenic coolers integrated with microsystems can provide low operating temperatures and significantly improve the performance of these systems (e.g., Q factor of micromechanical resonators[1] and sensitivity of chemical sensors[2]). Most current TE microcoolers[3–6] are of single stage, and a planar multistage cryogenic microcooler[1] is recently proposed to overcome the technical challenges of the pyramid design for Micro-Electro-Mechanical Systems (MEMS) fabrication processes, and it has the potential to reach lower temperatures than the single-stage design.

Fabrication of TE microcoolers is mainly based on thin or thick TE film techniques.[3,4,6] The most commonly used TE materials are telluride compounds, which have been studied extensively and are the commercialized TE cooling material choice near room temperature. Bulk Bi_2Te_3 and Sb_2Te_3 have high TE figure of merit Z_eT (around 1.0) [$Z_e=\alpha_S^2T/(\rho_e k)$, here α_S is the Seebeck coefficient, ρ_e is the electrical resistivity, and k is the thermal conductivity] near room temperature and can be fabricated as n- and p-type films to form a TE couple. A number of techniques have been used to fabricate Bi_2Te_3 and Sb_2Te_3 films, e.g., coevaporation,[7,8] cosputtering,[4,9] metal organic chemical vapor deposition,[10,11] molecular beam epitaxy (MBE),[12] and electroplating.[13] Some reported deposition techniques and TE properties of the resulting n-type and p-type TE films are shown in Table I. Here coevaporation is used because of relatively high film quality, short processing time, and compatibility with film micropatterning.

The growth conditions for coevaporated Bi_2Te_3 and Sb_2Te_3 thin films on glass and their room-temperature TE properties have been investigated.[7,8] Although the temperature dependence of bulk Bi_2Te_3 and Sb_2Te_3 crystals has been studied extensively,[14,15] the low-temperature TE properties of the coevaporated Bi_2Te_3 and Sb_2Te_3 thin films have rarely been reported. Because the design object of cryogenic microcoolers is to provide an operation temperature well below the room temperature (100–270 K), due to the strong temperature dependence of TE properties (α_S, ρ_e, and k), the low-temperature (100–270 K) characterization of these TE transport parameters is important for design and fabrication of microscale cryogenic TE coolers. Those low-temperature TE properties are also useful for the investigation of carrier transport in films.

In the fabrication of the micro-TE coolers, the TE films need to be micropatterned to form n-p couples using technique such as shadow mask or photolithography. The patterning technique also determines the substrate temperature limits (e.g., when using photoresists) and can affect the

a)Electronic mail: kaviany@umich.edu.

TABLE I. Reported deposition techniques and properties of n-Bi_2Te_3 and p-Sb_2Te_3/$(Bi_xSb_y)_2Te_3$ films.

Technique	Coevaporation				Cosputtering		Electroplating	MOCVD	
Reference	da Silva *et al.*[a]		Zou *et al.*[b]		Böttner *et al.*[c]		Lim *et al.*[d]	Giani *et al.*[e]	
Substrate	Glass		Glass		SiO_2/Si		Cu	Pyrex and Si	
TE materials	n-Bi_2Te_3	p-Sb_2Te_3	n-Bi_2Te_3	p-Sb_2Te_3	n-Bi_2Te_3	p-$(Bi,Sb)_2Te_3$	n-Bi_2Te_3	n-Bi_2Te_3	p-Sb_2Te_3
T_{sub} (K)	533	543	533/503[f]	503/463[f]	⋯	⋯	498		
α_S (μV/K)	−228	149	−228/−200 [f]	171/160[f]	−160	190	−60	−210	110
ρ_e ($\mu\Omega$ m)	28.3	12.5	13.0/12.9[f]	10.4/31.2[f]	16.3	14.3	10.0	9.0	3.5
α_S^2/ρ_e (mW/K^2 m)	1.84	1.78	4.0/3.10[f]	2.30/0.82[f]	1.57	2.53	0.36	4.90	3.46

[a]Reference 7.
[b]Reference 8.
[c]Reference 4.
[d]Reference 13.
[e]Reference 11.
[f]The results after the slash are for n-p film thermocouple (Ref. 8).

growth conditions for Bi_2Te_3 or Sb_2Te_3 films and their TE properties.

Here we report on the characterization of the TE transport properties, i.e., Seebeck coefficient, electrical conductivity, mobility, and Hall coefficient of coevaporated Bi_2Te_3 and Sb_2Te_3 films grown under our optimal coevaporation deposition conditions. We also discuss application of the shadow-mask micropatterning technique and explore its effects on film growth conditions and TE properties.

II. COEVAPORATION OF TE MATERIAL

The coevaporation system is shown in Fig. 1. Before deposition, a wafer was first cleaned using acetone, dried in nitrogen flow, and placed on a rotating wafer supporter. The chamber is then evacuated until the pressure reaches 10^{-7} torr. The substrate temperature was controlled between 423 and 573 K through radiation from a heater by adjusting its input electric power. In the deposition chamber, each of the elements (99.999% pure Te, Bi, and Sb shots) of the desired compound (from the Bi–Te or Sb–Te systems) was placed in a molybdenum boat. The deposition mass flux of each source was controlled by adjusting the individual power applied to the corresponding boats.

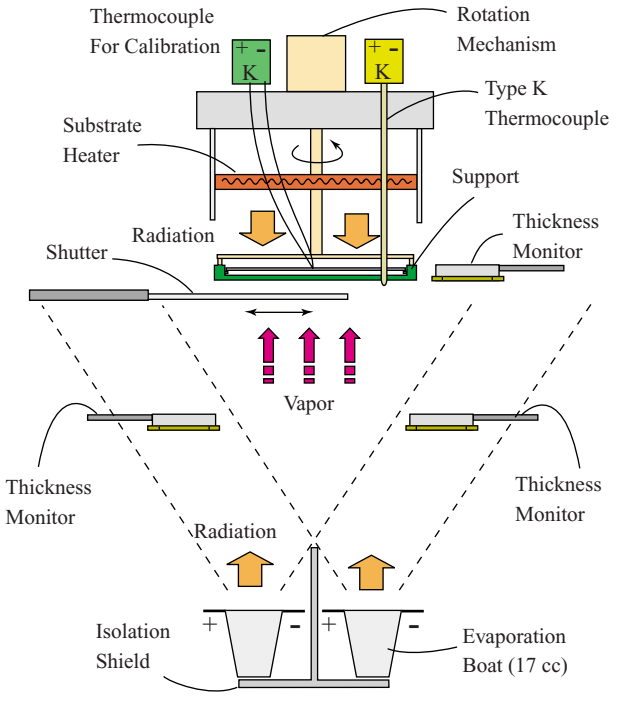

FIG. 1. (Color online) Schematic of coevaporation system.

The chamber pressure during the deposition was varied from 8×10^{-7} to 4×10^{-6} torr. The deposition rates of Sb and Bi were set to 1.0 Å/s, while the deposition rate of Te varied from 1.5 to 4.0 Å/s. The fluctuation in the deposition rate was controlled to within 10%. Energy Dispersive X-ray Analysis (EDX) analysis was made to verify the Bi(Sb)/Te ratio for the grown films and to control the composition of the films; x-ray diffraction was used for phase analysis.

Figure 2 shows the dependence of α_S and σ_e on the film thickness for Sb_2Te_3 films deposited under the optimal conditions. In the thickness range between 0.75 and 4 μm, no distinguishable correlation between the TE properties and film thickness was observed, so films with a thickness around 1 μm were used for characterization. This thickness is also closed to values used by da Silva *et al.*[7] and Zou *et al.*[8]

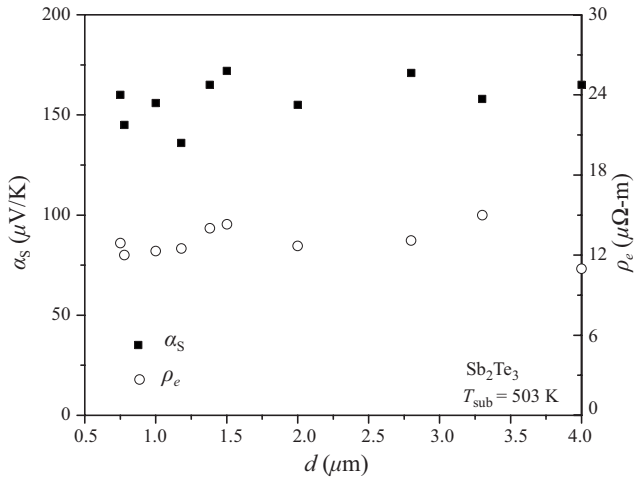

FIG. 2. Variation in Seebeck coefficient and electrical conductivity of Sb_2Te_3 films (deposited with T_{sub}=503 K and FR=3.0) with respect to the film thickness.

TABLE II. Comparison of the deposited best films on different substrates. The α_S^2/ρ_e data were measured at 300 K. The results before the slash are for Bi_2Te_3 and those latter are for Sb_2Te_3.

Substrate	Optimal T_{sub} (K)	Uniformity	Adherence	α_S^2/ρ_e (mW/K^2 m)	FR
Glass	533/503	Poor	Excellent	2.35/2.08 (center)	2.4/3.0
Si	<453	Good	Poor	···	~1.5/1.5
Si_3N_4/Si	500/483	Good	Poor	1.51/1.24	2.0/1.7
SiO_2/Si	533/503	Good	Good	2.30/1.98	2.4/3.0

A. Deposition condition

During the coevaporation, the important variables that can be controlled are substrate material, substrate temperature T_{sub}, and deposition flux ratio (FR). Their optimization is discussed below.

For the compatibility with conventional micromachining processing, we have tested the depositions on various substrates commonly used in micromachining processing including glass, silicon (Si), Si coated with silicon nitride (Si_3N_4/Si), and Si coated with silicon oxide (SiO_2/Si). Table II compares the films deposited on the different 4 in. substrates. Although glass substrate may result in the best adherence and film quality at the center, its low thermal conductivity leads to a large temperature variation across the surface and, in turn, a noticeable inhomogeneity (nonuniformity) in the TE properties. Also, to obtain high Z_e, the films are expected to be deposited at high temperatures (above 453 K),[7,8] but then the adherence of Bi_2Te_3 and Sb_2Te_3 films (especially Sb_2Te_3 films) to the Si and Si_3N_4/Si substrates becomes rather poor. Above 453 K, no adherence of Sb_2Te_3 to the Si substrates was found. However, the SiO_2/Si substrate produces tightly adhered relatively high quality uniform films at high temperature. In addition, the SiO_2/Si substrate is electrically insulating in the intended operational range, which is desired in the planar multistage design.[1] Therefore, SiO_2/Si substrates are the preferred choice here for the coevaporation.

Strong dependence of the Te vapor atom sticking coefficient on the substrate temperature T_{sub} and elemental FR of the TE species (Te:Bi/Sb) has been observed by Mzerd *et al.*[16] in the depositions on Si substrates using MBE. However, in coevaporation deposition, progressive loss of Te in both Bi_2Te_3 and Sb_2Te_3 films was found when T_{sub} was above 473 K, which is different from the steplike behavior found at around 573 K in MBE by Mzerd *et al.*[16] This deviation is probably due to the difference in the kinetic energy of Te atoms and the substrate surface force that they experience. Since the sublimation temperature of tellurium is around 473 K at 1.0×10^{-5} torr, it is reasonable to attribute the loss of Te to its resublimation at high temperatures. Figure 3 shows the variation in the measured composition ratio of Te/Bi(Sb) of the films with respect to FR at the optimal T_{sub}. At T_{sub}=503 K, when the FR is between 2.0 and 3.0, the atomic concentrations of Sb and Te do not change significantly, indicating the resublimation of tellurium. However, when the FR is larger than 3.5, the concentration of Te is significantly larger, indicating a net condensation of Te on the substrate. This is verified by the x-ray diffraction patterns, in which Te peaks were observed, while no evidence of SbTe was observed (similar to those reported in Ref. 16). Similar phenomena occur for Bi_2Te_3, and the dependence of compositions on FR is even stronger, indicating that the resublimation of Te is less significant for Bi_2Te_3 films.

The substrate temperature T_{sub} also affects the grain structure of TE films. Figures 4(a)–4(c) are the scanning electron microscopy (SEM) micrographs of Bi_2Te_3 films deposited on the SiO_2/Si substrates at 453, 533, and 556 K, respectively; Figs. 4(a)–4(c) are for Sb_2Te_3 films deposited on the same substrates at 453, 503, and 524 K, respectively. The results show that for low T_{sub}, the grain boundary blurs and the grain size is small. As T_{sub} increases, the grain size as well as α_S increases, while the ρ_e decreases. These are similar to the results reported in Ref. 7. However, if T_{sub} is high ($\geq$482 K), the film becomes more grainy (due to resublimation of Te). If T_{sub} increases further, resublimation counteracts the effects of larger grain size and results in increased ρ_e. If T_{sub} is too high, TE films may even become discontinuous. Our optimal T_{sub} for coevaporated Bi_2Te_3 and Sb_2Te_3 films (listed in Table III) were obtained by comparing the power factor α_S^2/ρ_e of films of near stoichiometric compositions deposited at different T_{sub}. Our optimal substrate temperatures for Bi_2Te_3 and Sb_2Te_3 films are 535 and 503 K (listed in Table III), respectively. These are close to those reported by Zou *et al.*[8] but different from those reported by da Silva *et al.*[7]

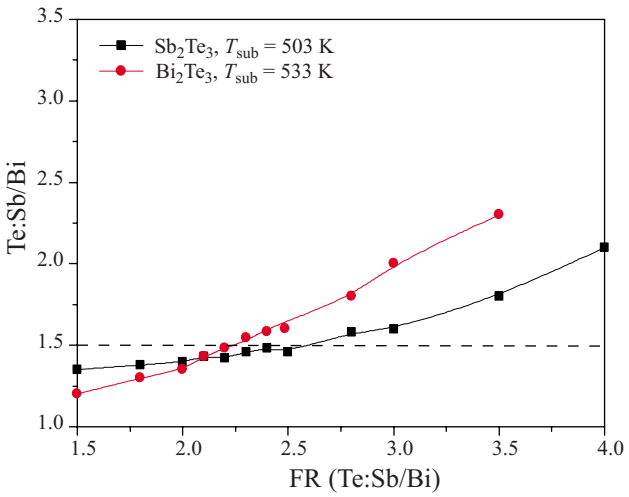

FIG. 3. (Color online) Variation in film composition ratio Te/Bi(Sb) with respect to FR at the optimal T_{sub}, i.e., T_{sub}=533 K for Bi_2Te_3 and 503 K for Sb_2Te_3.

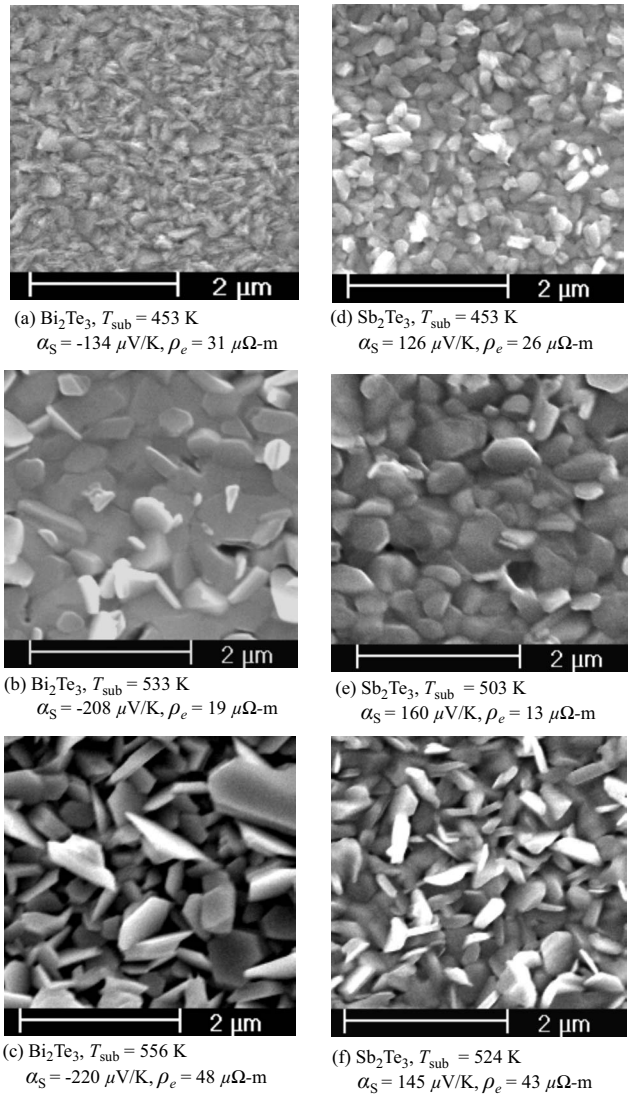

FIG. 4. [(a)–(c)] SEM micrographs of the Bi_2Te_3 films deposited at different substrate temperatures with a FR of 2.4. [(d)–(f)] SEM micrographs of the Sb_2Te_3 films deposited at different substrate temperatures with a FR of 3.0.

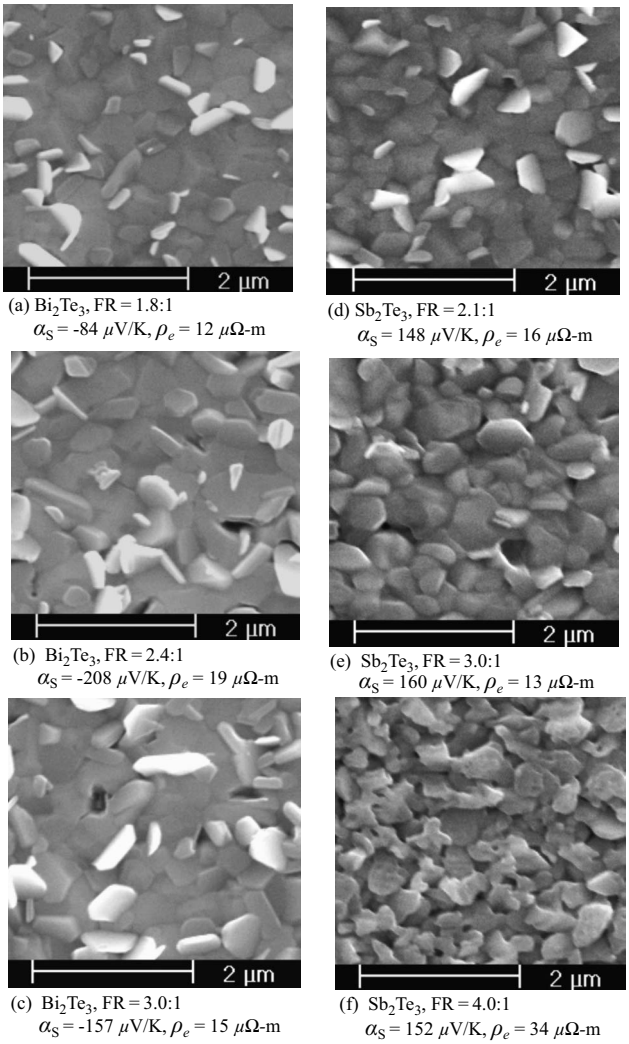

FIG. 5. [(a)–(c)] SEM micrographs of the Bi_2Te_3 films deposited with different evaporation FRs at 533 K. [(d)–(f)] SEM micrographs of Sb_2Te_3 films deposited with different evaporation FRs at 503 K.

Figures 5(a)–5(c) are the SEM micrographs of Bi_2Te_3 films deposited on SiO_2/Si substrates with different FRs at 533 K, and Figs. 5(d)–5(f) are for Sb_2Te_3 films on the same substrates with different FRs at 503 K. When FR increases, the grain size of both films increases at first, resulting in a lower ρ_e and a higher α_S. When the FR is set too large, for Bi_2Te_3 films the atomic concentration of Te becomes larger and both α_S and ρ_e decrease. Note that for Sb_2Te_3, a large FR may even reduce the grain size and α_S and increase ρ_e, which is believed to be due to the strong resublimation of Te, as shown in Fig. 3. Our optimal coevaporation FR was obtained by evaluating the power factor α_S^2/ρ_e of films deposited on the SiO_2/Si substrates at the optimal T_{sub}, which is found to be 3.0 for Sb_2Te_3 and 2.4 for Bi_2Te_3 (also shown in Table III). This result is different from FR=2.2 for both Bi_2Te_3 and Sb_2Te_3 films reported in Ref. 8.

Our optimal coevaporation conditions and the TE properties of the resulting TE films are listed in Table III. At room temperature, the highest power factors achieved were 2.30 $mW/K^2\,m$ for *n*-type Bi_2Te_3 films and 1.98 $mW/K^2\,m$ for *p*-type Sb_2Te_3 films. The measured power factor data for both films are better than the corresponding results in Ref. 7; the obtained results for Sb_2Te_3 films are also better than the result for *n-p* film couples in Ref. 8; however, our Bi_2Te_3 films have a lower power factor than those in Ref. 8, as shown in Table I.

TABLE III. Obtained optimal coevaporation conditions for Bi_2Te_3 and Sb_2Te_3 films and their room-temperature TE performance.

Film	T_{sub} (K)	FR	α_S ($\mu V/K$)	ρ_e ($\mu\Omega$ m)	α_S^2/ρ_e (mW/K^2 m)	n_c ($10^{25}/m^3$)	μ (10^{-4} m^2/V s)
Bi_2Te_3	535	2.4	−208	18.8	2.30	3.07	113
Sb_2Te_3	503	3.0	160	12.9	1.98	1.35	303

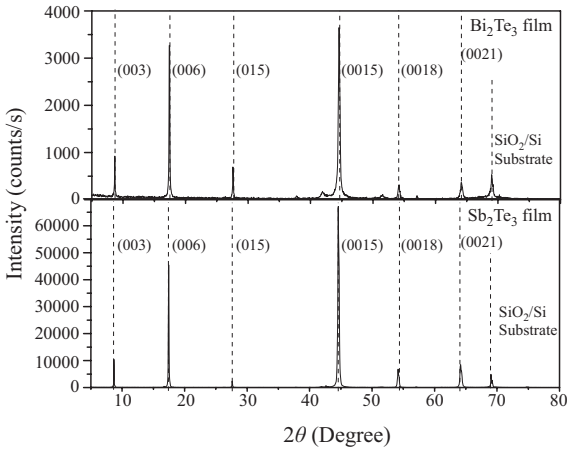

FIG. 6. X-ray diffraction spectrum for optimal Bi_2Te_3 and Sb_2Te_3 films.

B. X-ray diffraction pattern

Figure 6 shows the x-ray diffraction spectrum of the optimized Sb_2Te_3 and Bi_2Te_3 films. The dashed lines in the figures are the x-ray diffraction spectra of powdered Bi_2Te_3 and Sb_2Te_3 single crystal. The peaks of the two spectra agree with each other. Also, the main peaks are very sharp and no pattern other than those of Sb_2Te_3 or Bi_2Te_3 appears, indicating that the measured films have only a single crystalline phase of Bi_2Te_3 or Sb_2Te_3. Moreover, it is apparent that for both Bi_2Te_3 and Sb_2Te_3 films only $(0,0,n)$ peaks are significant, indicating a preference for the *c*-axis orientation. This orientation preference is also apparent in Fig. 4 and is in agreement with the findings in Ref. 7.

III. LOW-TEMPERATURE TE PROPERTIES OF Bi_2Te_3 AND Sb_2Te_3

Liquid nitrogen and helium were used to cool the cryostat down for the low-temperature characterization of TE properties. α_S and ρ_e were first measured using the configuration described in Ref. 7, from 100 to 300 K. Then, a four-probe ac technique adopting a modified probe of a Magnetic Property Measurement System (MPMS) (Quantum Design) was used to obtain the Hall coefficient R_H, ρ_e, and the mobility μ_e from 5 to 300 K. The deviation of the two sets of measured ρ_e is very small (less than 8%) in the temperature range where they overlap (100–300 K).

Figures 7(a) and 7(b) show the temperature dependence of the Hall coefficients R_H of the coevaporated Bi_2Te_3 and Sb_2Te_3 films, respectively. The experimental data[15,19] for bulk materials are also shown. The coevaporated Bi_2Te_3 and Sb_2Te_3 films are *n*- and *p*-type, respectively. Below 20 K, for both Bi_2Te_3 and Sb_2Te_3 films, R_H do not change noticeably, a behavior in saturation regime. However, unlike a doped crystalline semiconductor, both samples do not demonstrate a freeze-out regime, indicating impurity-band conduction.[17] When $T>20$ K, R_H of Bi_2Te_3 decreases with increasing temperature (due to thermal excitation). In contrast, R_H of bulk Bi_2Te_3 is a constant below 150 K and decreases at higher temperatures. This difference may also be due to impurity band. Above 200 K, R_H of Bi_2Te_3 film is very close to that of bulk materials.[15] For Sb_2Te_3, R_H first slightly decreases when the temperature rises from 20 to around 70 K, and then increases when the temperature rises further. This anomalous temperature dependence of R_H is believed to be related to the change in the degeneracy correction factor.[17] Similar results have been found for doped bulk As_2Te_3 crystals[18] and Sb_2Te_3 single crystal and its alloys.[19] Near room temperature, R_H is much higher than that of bulk materials,[19] indicating a lower carrier concentration.

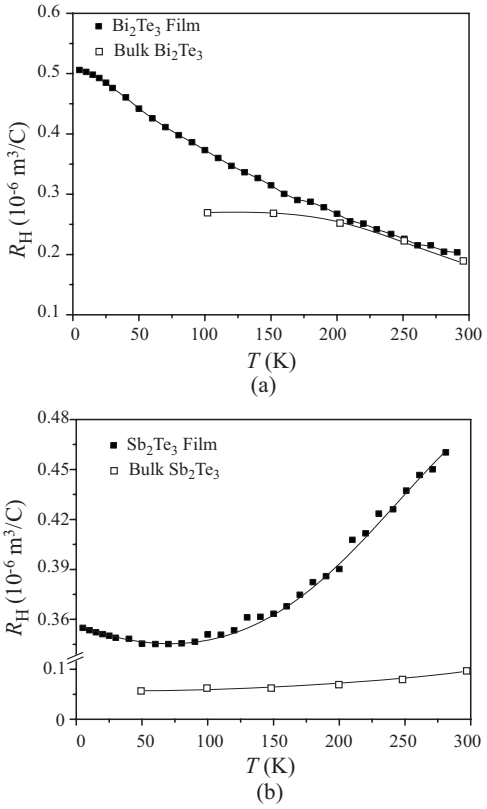

FIG. 7. Temperature dependence of the Hall coefficients of the optimal (a) Bi_2Te_3 and (b) Sb_2Te_3 films. The experimental results for bulk materials (Refs. 15 and 19) are also shown.

Figures 8(a) and 8(b) show the measured ρ_e and μ_e of the Bi_2Te_3 and Sb_2Te_3 films over the temperature range from 1 to 300 K. The experimental ρ_e and μ_e (derived from ρ_e and R_H) for bulk materials[15,19] are also shown. As shown in Fig. 8(a) for Bi_2Te_3, ρ_e almost remains constant below 20 K and gradually becomes larger when $T>20$ K; above 180 K, ρ_e becomes a linear function of temperature. ρ_e of Sb_2Te_3 shows a different temperature dependence, although it also changes little below 20 K. As shown in Fig. 8(b), ρ_e of Sb_2Te_3 thin films varies much slower with increasing temperature; the linear relation with temperature only appears above 250 K, and from 20 to 300 K, ρ_e changes by a factor of 2, compared with a factor of 6 for the Bi_2Te_3 film. Figures 8(a) and 8(b) show that μ_e of both the Bi_2Te_3 and Sb_2Te_3 films at low temperature ($T<20$ K) vary slowly with temperature ($\mu_e \propto T^{-0.03}$), which is believed to result from the combination of ionized-impurity scattering and alloy scattering. Above 100 K, μ_e of the Bi_2Te_3 film shows a dependence of $T^{-1.75}$, indicating that the scattering of electrons is mainly due to the acoustic-mode lattice scattering, which is similar to the behavior of bulk materials; however, μ_e of the Sb_2Te_3

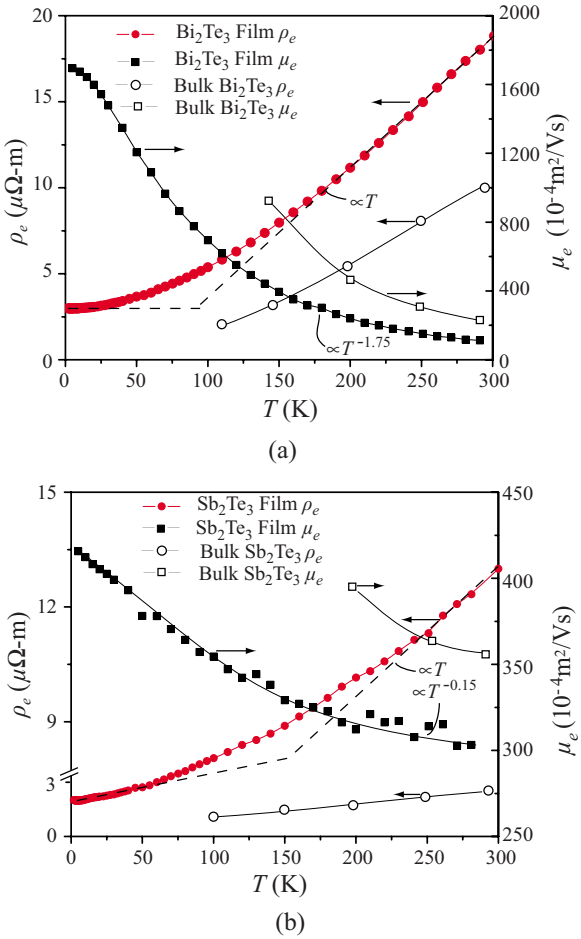

FIG. 8. (Color online) Temperature dependence of the electrical resistivity and the mobility of the deposited (a) Bi_2Te_3 and (b) Sb_2Te_3 films. The experimental results for bulk materials (Refs. 15 and 19) are also shown.

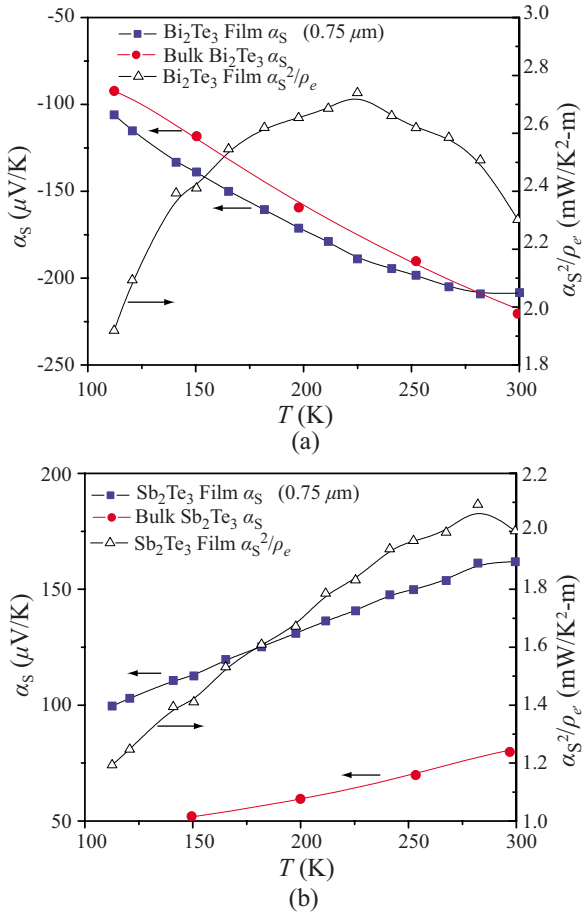

FIG. 9. (Color online) Temperature dependence of the Seebeck coefficient and power factor of the deposited (a) Bi_2Te_3 and (b) Sb_2Te_3 films. The Seebeck coefficients of bulk Bi_2Te_3 and Sb_2Te_3 films reported in the literature (Refs. 9 and 19) are also shown.

film illustrates a dependence of $T^{-0.15}$, suggesting the scattering by both acoustic-mode lattice scattering and ionized impurity scattering.[20] As shown in Figs. 8(a) and 8(b), μ_e of Bi_2Te_3 films is almost 40% of that of bulk materials, while for Sb_2Te_3 films, μ_e of the films and bulk materials are close. Near room temperature, ρ_e of both the Bi_2Te_3 and Sb_2Te_3 films are much higher than the values for bulk materials.[15,19] From the analysis of R_H and μ_e, we note that, for Bi_2Te_3 films, their higher ρ_e mainly results from a lower mobility, while for Sb_2Te_3 films, their higher ρ_e is mainly due to a lower carrier concentration.

Figures 9(a) and 9(b) show the variation in α_S and α_S^2/ρ_e from 100 to 300 K. For both the Bi_2Te_3 and Sb_2Te_3 films, the absolute value of α_S increases with increasing temperature. For Bi_2Te_3 films, α_S is very close to that of the bulk single crystals[9] (for bulk single crystals, α_S is nearly isotropic[21]). For Sb_2Te_3 films, however, α_S is much higher than that of pure bulk single crystals.[19] This relates to the carrier concentration n_c. For Bi_2Te_3, n_c of the films is close to that of bulk single crystals, while for Sb_2Te_3, according to Fig. 7(b), n_c of the film is only 1/5–1/4 of that of the bulk single crystals. According to the relation $\alpha_S \simeq k_B/e_c[-\ln(n_c)+\cdots]$,[22] the carrier concentration difference of a factor of 1/4 will lead to a 110 μV/K difference in α_S, in good agreement with the difference (around 90 μV/K) shown in Fig. 9(b).

Figures 9(a) and 9(b) also show that, for Bi_2Te_3 films, α_S^2/ρ_e reaches its maximum (2.7 $\mathrm{mW/K^2\,m}$) at around 225 K, while the maximum for Sb_2Te_3 (2.1 $\mathrm{mW/K^2\,m}$) is around 280 K. This temperature difference is mainly due to the different temperature dependences of ρ_e.

IV. TE FILM MICROPATTERNING

Various methods have been used to micropattern films, e.g., chemical etching[7] and photoresist lift-off (dry etching).[4] When photoresists are used for patterning both *n*-type and *p*-type films on the same wafer, the substrate temperature is limited and the TE properties may be worse than those optimal values for individual deposition.[7] Böttner *et al.*[4] patterned the *n*-type and *p*-type films on two wafers separatively and then bonded the two wafers together. The applications of shadow mask techniques for TE film patterning have not yet been reported. Here we adopted the common shadow mask technique because of its simplicity, compatibility with high substrate temperature for film deposition, and the ability to micropattern both *n*-type and *p*-type films on the same wafer. One fabricated silicon shadow mask is shown in Figs. 10(a) and 10(b). The patterned Bi_2Te_3 deposited at 533 K is shown as an example in Fig. 10(c). The deposited patterns have dimensions very close to those of the openings on the shadow mask. The smallest pattern has a dimension of 23

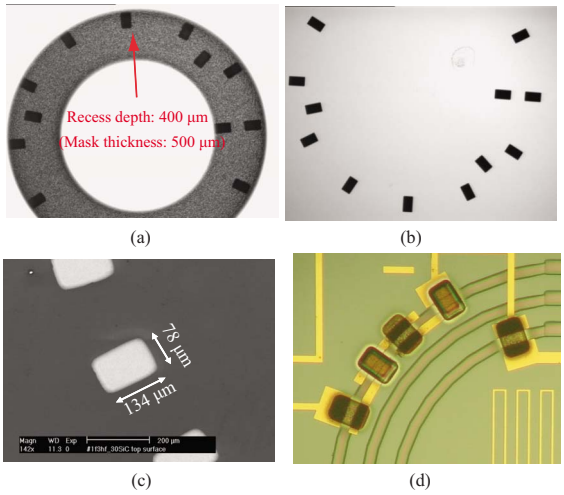

FIG. 10. (Color online) (a) Top view of the fabricated Si shadow mask. (b) Bottom view of the fabricated Si shadow mask. (c) Deposited Bi_2Te_3 patterns using the shadow mask. (d) Aligned Bi_2Te_3 and Sb_2Te_3 film patterns.

$\times 75\ \mu m^2$. These tests show that the shadow mask can be used to pattern the films to a small dimension of around $20-30\ \mu m$.

To make a TE cooler, both the *n*-type (Bi_2Te_3) and *p*-type (Sb_2Te_3) patterned films should be deposited, requiring a dual deposition. Since our optimal coevaporation deposition of Bi_2Te_3 films is found with a substrate temperature of 533 K, which is higher than that for Sb_2Te_3 deposition, to avoid any damage to the film deposited first, Sb_2Te_3 was deposited following the deposition of Bi_2Te_3. The dual deposition needs two separate shadow masks (one for Bi_2Te_3 and the other for Sb_2Te_3). First, the shadow mask for Bi_2Te_3 was aligned with the substrate under an optical microscope. Then the shadow mask and the substrate were fixed together by stainless steel screws. This shadow mask/substrate was placed in the deposition chamber and a layer of Bi_2Te_3 film was deposited with $T_{sub}=533$ K (note that the shadow mask may raise the substrate temperature by around 10 K, and before the deposition, a careful temperature recalibration should be carried out). After this deposition, the heater was turned off and the substrate was left in the chamber until it cooled down to room temperature. Then the shadow mask was removed and the other shadow mask for Sb_2Te_3 deposition was carefully mounted. Following the same deposition procedure for Sb_2Te_3 described in Sec. II A, we obtained Bi_2Te_3 and Sb_2Te_3 patterns shown in Fig. 10(d).

When fabricating the *n-p* film couples, the TE properties of the films may possibly change because the deposition conditions for Bi_2Te_3 and Sb_2Te_3 films are different.[8] To examine the effects of this dual deposition on the TE properties of the deposited films, we measured the TE properties of large TE patterns deposited in a single deposition using the two shadow masks separately, and the results were similar to those deposited without shadow masks (deviation is within 15%). We also measured the room-temperature TE properties of the large Bi_2Te_3 patterns before and after the secondary deposition for Sb_2Te_3; the difference is less than 5% for both ρ_e and α_S (within the measurement error), that is, no significant changes in the TE properties of Bi_2Te_3 are observed, suggesting suitability of shadow mask technique for TE film micropatterning.

V. SUMMARY AND CONCLUSIONS

We examined the growth conditions for coevaporated Bi_2Te_3 and Sb_2Te_3 films including the effects of substrate material, substrate temperature, and FR. Good film quality was obtained with our optimal deposition conditions and compared with the data using the same coevaporation method in the literature.[7,8] The low-temperature TE properties of the optimal coevaporated Bi_2Te_3 and Sb_2Te_3 films were characterized over a wide temperature range (100–300 K for α_S, 5–300 K for ρ_e, μ_e, and R_H). All the TE properties of both Bi_2Te_3 and Sb_2Te_3 films strongly depend on the operation temperature (Bi_2Te_3 films show a stronger temperature dependence), which must be considered in the design of cryogenic microcoolers. The maximum power factor α_S^2/ρ_e of coevaporated films are both achieved below room temperature, i.e., 2.7 $mW/K^2\,m$ for Bi_2Te_3 at $T=220$ K and 2.1 $mW/K^2\,m$ for Sb_2Te_3 at $T=280$ K. The analysis of the mobility μ_e shows that the major scattering mechanism for Bi_2Te_3 films near room temperature is the acoustic-phonon scattering, and that for Sb_2Te_3 is a combination of the acoustic-phonon scattering and ionized-impurity scattering. The lower performance of the coevaporated films mainly results from a higher ρ_e. For Bi_2Te_3 films, the high ρ_e is mainly due to a low μ_e, while for Sb_2Te_3 films, it is due to a low carrier concentration.

Micropatterned TE *n*-Bi_2Te_3/*p*-Sb_2Te_3 couples were fabricated on SiO_2/Si substrates using dual deposition procedure adopting the shadow mask technique under the optimized coevaporation conditions. Using the shadow mask technique has negligible effects on the TE film properties and makes it suitable for the manufacture of micro-TE systems.

ACKNOWLEDGMENTS

This project is supported by the MCC program of DARPA under Grant No. W31P4Q-06-1-001.

[1] A. Gross, B. L. Huang, G. S. Hwang, C. Lawrence, N. Ghafouri, S. W. Lee, H. Kim, C. Uher, M. Kaviany, and K. Najafi, IEEE 21st International Conference on Microelectromechanical Systems, 2008 (unpublished), p. 840–843.
[2] L. W. da Silva and M. Kaviany, Int. J. Heat Mass Transfer **47**, 2417 (2004).
[3] G. Min and D. M. Rowe, Solid-State Electron. **43**, 923 (1999).
[4] H. Böttner, J. Nurnus, A. Gavrikov, G. Kühner, M. Jägle, C. Kunzel, D. Eberhard, G. Plescher, A. Schubert, and K. H. Schlereth, J. Microelectromech. Syst. **13**, 414 (2004).
[5] L. W. da Silva and M. Kaviany, J. Microelectromech. Syst. **14**, 1110 (2005).
[6] L. M. Goncalves, J. Nurnus, C. Couto, P. Alpuim, G. Min, D. M. Rowe, and J. H. Correia, J. Microelectromech. Syst. **17**, S168 (2007).
[7] L. W. da Silva, M. Kaviany, and C. Uher, J. Appl. Phys. **97**, 114903 (2005).
[8] H. Zou, D. M. Rowe, and S. G. K. Williams, Thin Solid Films **408**, 270 (2002).
[9] D.-H. Kim, E. Byon, G.-H. Lee, and S. Cho, Thin Solid Films **510**, 148 (2006).
[10] R. Venkatasubramanian, T. Colpitts, E. Watko, M. Lamvik, and N. El-Masry, J. Cryst. Growth **170**, 817 (1997).

[11]A. Giani, A. Boulouz, F. Pascal-Delannoy, A. Foucaran, E. Charles, and A. Boyer, Mater. Sci. Eng., B **64**, 19 (1999).
[12]J. Nurnus, H. Beyer, H. Bottner, and A. Lambrecht, 5th European Workshop on Thermoelectrics, 1999 (unpublished), Vol. 1, p. 1.
[13]J. R. Lim, G. J. Synder, C.-K. Huang, J. A. Herman, M. A. Ryan, and J. P. Fleurial, Proceedings of the 21st International Conference on Thermoelectrics, 2002 (unpublished), pp. 535–539.
[14]H. J. Goldsmid, *Thermoelectric Refrigeration* (Plenum, New York, 1964).
[15]J. P. Fleurial, L. Gailliard, R. Triboulet, H. Scherrer, and S. Scherrer, J. Phys. Chem. Solids **49**, 1237 (1988).
[16]A. Mzerd, D. Sayah, G. Brun, J. C. Tedenac, and A. Boyer, J. Mater. Sci. Lett. **14**, 194 (1995).
[17]E. M. Conwell, Phys. Rev. **103**, 51 (1956).
[18]T. C. Harman, B. Paris, S. E. Miller, and H. L. Goering, J. Phys. Chem. Solids **2**, 181 (1957).
[19]C. Drasar, M. Steinhart, P. Lostak, H.-K. Shin, J. S. Dyck, and C. Uher, J. Solid State Chem. **178**, 1301 (2005).
[20]J. Singh, *Electronic and Optoelectronic Properties of Semiconductor Structures* (Cambridge, New York, 2003).
[21]T. J. Scheidemantel, C. Ambrosch-Draxl, T. Thonhauser, J. V. Badding, and J. O. Sofo, Phys. Rev. B **68**, 125210 (2003).
[22]G. D. Mahan, Solid State Phys. **51**, 82 (1997).